

GAZİ

JOURNAL OF ENGINEERING SCIENCES

Comparison of Turbulence Models and Wall Layer Mesh in a Solar Air Heater

Özgür Erol^a

Submitted: 22.02.2022 Revised: 04.08.2022 Accepted: 09.08.2022 doi:10.30855/gmbd.0705016

ABSTRACT

Keywords: Turbulence models, Wall layer mesh structure, Solar air heater

^a Başkent University,
Faculty of Engineering,
Dept. of Mechanical Engineering
06790 - Ankara, Türkiye
Orcid: 0000-0002-8824-4290
e-mail: erol@baskent.edu.tr

*Corresponding author:
erol@baskent.edu.tr

Turbulence models and the wall layer mesh thickness that are given to the walls are two important parameters for the solution of the fluid mechanics problems in Computational Fluid Dynamics. For different problems in engineering, different turbulence models are efficient. Also the thickness of the wall layer, which is determined before the solution, is another parameter which affects the result of the solution for a selected turbulence model. In this study, three turbulence models, which are k-ε, Renormalization-Group k-ε (RNG) and Low Reynolds Number k-ε models, were compared for 3, 6 and 9 levels of wall layer on a flat solar air heater. The results were compared with the results given in the literature. In the analysis of the solar air heater, solar radiation calculations were made for a better simulation. According to the comparison of the results that were acquired from the CFD solutions and the results in the literature, Renormalization-Group k-ε using six wall layers is found to be the best method and wall layer thickness among the alternatives that were investigated.

Hava Akışkanlı Bir Güneş Toplacında Türbülans Modellerinin ve Duvar Tabaka Ağ Yapısının Karşılaştırması

ÖZ

Türbülans modelleri ve duvarlara atanan duvar tabaka ağ kalınlığı, hesaplamalı akışkanlar dinamiğinin kullanıldığı akış problemlerinin iki önemli parametresini oluşturmaktadır. Mühendislikteki farklı problemler için farklı türbülans modelleri etkin bir şekilde kullanılmaktadır. Ayrıca duvar ağ yapısı oluşturulurken belirlenen duvar tabaka ağ kalınlığı da seçilmiş olan türbülans modelinden elde edilecek sonucu etkileyen bir parametredir. Bu çalışmada, hava akışkanlı bir güneş toplacı için üç farklı türbülans modeli, k-ε, RNG k-ε ve düşük Reynolds sayısı için k-ε modelleri, 3, 6 ve 9 kademe duvar tabaka ağ kalınlıklarında incelenmiştir. Elde edilen sonuçlar incelendiğinde, incelemesi yapılan modeller arasındaki en iyi sonucun altı seviye duvar tabaka ağ yapısına sahip RNG metodu olduğu görülmektedir.

Anahtar Kelimeler: Türbülans modelleri, Duvar tabaka ağ yapısı, Güneş toplacı

1. Introduction

Computational Fluid Dynamics (CFD) methods are powerful tools in the design of the fluid systems in various places of the industry and science. They are relatively cheap and fast tools for the scientists and engineers to make decisions and direct their research or design to an appropriate way without spending high amounts of money and effort. One of the drawbacks of CFD methods is that one can get any result if inappropriate methods and parameters are selected for the definition of the problem. Selection of the turbulence model is one of the most important parameter among these parameters. The accuracy of the simulation changes with the turbulence model that was chosen.

Different kinds of turbulence models are used for different kinds of CFD problems. In the literature, there are studies which compare these turbulence models for different types of problems. Mishra and Aharwal [1] made a review on the turbulence models used in the cold storage air flow problems. Bartosiewicz et. al. [2], Gagan et. al. [3] and Varga et. al. [4] made comparative studies on the selection of turbulence models for steam and gas ejectors.

Also for different cases in aeronautics, turbulence model comparison studies were made by different researchers, such as for the supersonic separated flows [5], low Reynolds number flow on delta wings [6] or flow on different airfoils [7].

Turbulence model comparisons were also made for turbomachinery applications, which have rotating parts like the studies made by Bharanitharan and Sentilkumar [8], Tog et.al. [9], Gibson et. al. [10] and Han and Huachen [11]. Also turbulence models were compared for the vertical-axis turbine applications like the studies made by Rezaeiha et. al. [12], Meana-Fernandez [13], Marsh et. al. [14].

Nuclear energy and various industrial applications are also application areas for CFD and turbulence model comparisons were also made in the literature, such as Kim et.al. [15], Guardo et.al. [16], Brown et.al. [17] and Mirzaei et.al. [18].

Wall layer mesh thickness is also a parameter that has to be defined before the simulation according to the turbulence model that is selected. Wall layer parameter adds elements to the solid-fluid border and produces a smooth and appropriate mesh distribution, which is critical for the solution [19]. Therefore assessment of the thickness of the wall layer for a particular turbulence model and geometry is an important factor in the solution of the problem.

In the literature, different CFD studies were made for various solar air heater problems and geometries. Very close solutions with respect to the experimental data can be found by using these methods, especially with radiation calculations. In their study, Vivekanandan et. al. made experimental and CFD investigation of the flow in a solar air heater [20]. Singh et. al. [21, 22], numerically investigated the performance of a solar air heaters coupled with buildings. They also [23] used CFD methods to estimate the performance of a curved double-pass solar air heater. The flow characteristics and performance analysis of different types of rib geometries used in the solar air heaters [24-27] were made by using the numerical methods.

In this study, three turbulence models, standard $k-\varepsilon$ model ($k-\varepsilon$), Renormalization group $k-\varepsilon$ (RNG) and Low Reynolds $k-\varepsilon$ (LowRe) models with 3 (prefix 3), 6 (prefix 6) and 9 (prefix 9) wall layer cell levels were compared for a flat plate solar air heater (SAH) problem. The problem is defined by using the experimental flat plate SAH study made by Kalaiarasi et. al. [28]. Test cases were solved by using Autodesk CFD software using solar radiation calculations.

2. Numerical Model

In this study, steady state flow simulations for a SAH were made by using Autodesk CFD software, which solves Navier-Stokes Equations of continuity, momentum and energy equations using Finite Element Method [29, 30].

Continuity;

$$\frac{\partial \rho}{\partial t} + \frac{\partial \rho U}{\partial x} + \frac{\partial \rho V}{\partial y} + \frac{\partial \rho W}{\partial z} = 0 \quad (1)$$

x-, y- and z-Momentum;

$$\rho \frac{\partial U}{\partial t} + \rho U \frac{\partial U}{\partial x} + \rho V \frac{\partial V}{\partial y} + \rho W \frac{\partial W}{\partial z} = \rho g_x - \frac{\partial p}{\partial x} + \frac{\partial}{\partial x} \left(2(\mu + \mu_t) \frac{\partial U}{\partial x} \right) + \frac{\partial}{\partial y} \left[(\mu + \mu_t) \left(\frac{\partial U}{\partial y} + \frac{\partial V}{\partial x} \right) \right] + \frac{\partial}{\partial z} \left[(\mu + \mu_t) \left(\frac{\partial U}{\partial z} + \frac{\partial W}{\partial x} \right) \right] + S_\omega + S_{DR} \quad (2)$$

$$\rho \frac{\partial V}{\partial t} + \rho U \frac{\partial V}{\partial x} + \rho V \frac{\partial V}{\partial y} + \rho W \frac{\partial V}{\partial z} = \rho g_y - \frac{\partial p}{\partial y} + \frac{\partial}{\partial x} \left[(\mu + \mu_t) \left(\frac{\partial U}{\partial y} + \frac{\partial V}{\partial x} \right) \right] + \frac{\partial}{\partial y} \left(2(\mu + \mu_t) \frac{\partial V}{\partial y} \right) + \frac{\partial}{\partial z} \left[(\mu + \mu_t) \left(\frac{\partial V}{\partial z} + \frac{\partial W}{\partial y} \right) \right] + S_\omega + S_{DR} \quad (3)$$

$$\rho \frac{\partial W}{\partial t} + \rho U \frac{\partial W}{\partial x} + \rho V \frac{\partial W}{\partial y} + \rho W \frac{\partial W}{\partial z} = \rho g_z - \frac{\partial p}{\partial z} + \frac{\partial}{\partial x} \left[(\mu + \mu_t) \left(\frac{\partial U}{\partial z} + \frac{\partial W}{\partial x} \right) \right] + \frac{\partial}{\partial y} \left[(\mu + \mu_t) \left(\frac{\partial V}{\partial z} + \frac{\partial W}{\partial y} \right) \right] + \frac{\partial}{\partial z} \left(2(\mu + \mu_t) \frac{\partial W}{\partial z} \right) + S_\omega + S_{DR} \quad (4)$$

Energy;

$$\rho C_p \frac{\partial T}{\partial t} + \rho C_p U \frac{\partial T}{\partial x} + \rho C_p V \frac{\partial T}{\partial y} + \rho C_p W \frac{\partial T}{\partial z} = \frac{\partial}{\partial x} \left((k + k_t) \frac{\partial T}{\partial x} \right) + \frac{\partial}{\partial y} \left((k + k_t) \frac{\partial T}{\partial y} \right) + \frac{\partial}{\partial z} \left((k + k_t) \frac{\partial T}{\partial z} \right) + q_v \quad (5)$$

where U, V and W are average velocities, SDR is the distributed resistance term, S_ω is the source term for the rotating flow and q_v is the volumetric heat source term. Also, μ_t and k_t terms given in the equations are defined as the eddy viscosity and eddy conductivity, respectively.

For the k- ϵ turbulence models that were examined in this study, two different equations of Turbulent Kinetic Energy (TKE) and Turbulent Energy Dissipation (TED) equations were added to the solution of the Navier-Stokes equations. There are slight differences in these equations according to the turbulence model that is used.

The k- ϵ turbulence model and the RNG model, which are high Reynolds number methods, use the same equations, except some constant values. In these models, TKE and TED equations are [31];

$$\rho \frac{\partial K}{\partial t} + \rho U \frac{\partial K}{\partial x} + \rho V \frac{\partial K}{\partial y} + \rho W \frac{\partial K}{\partial z} = \frac{\partial}{\partial x} \left[\left(\frac{\mu_t}{\sigma_K} \right) \frac{\partial K}{\partial x} \right] + \frac{\partial}{\partial y} \left[\left(\frac{\mu_t}{\sigma_K} \right) \frac{\partial K}{\partial y} \right] + \frac{\partial}{\partial z} \left[\left(\frac{\mu_t}{\sigma_K} \right) \frac{\partial K}{\partial z} \right] - \rho \epsilon + \mu_t \left[2 \left(\frac{\partial U}{\partial x} \right)^2 + 2 \left(\frac{\partial V}{\partial y} \right)^2 + 2 \left(\frac{\partial W}{\partial z} \right)^2 + \left(\frac{\partial U}{\partial y} + \frac{\partial V}{\partial x} \right)^2 + \left(\frac{\partial U}{\partial z} + \frac{\partial W}{\partial x} \right)^2 + \left(\frac{\partial V}{\partial z} + \frac{\partial W}{\partial y} \right)^2 \right] \quad (6)$$

$$\rho \frac{\partial \epsilon}{\partial t} + \rho U \frac{\partial \epsilon}{\partial x} + \rho V \frac{\partial \epsilon}{\partial y} + \rho W \frac{\partial \epsilon}{\partial z} = \frac{\partial}{\partial x} \left[\left(\frac{\mu_t}{\sigma_\epsilon} \right) \frac{\partial \epsilon}{\partial x} \right] + \frac{\partial}{\partial y} \left[\left(\frac{\mu_t}{\sigma_\epsilon} \right) \frac{\partial \epsilon}{\partial y} \right] + \frac{\partial}{\partial z} \left[\left(\frac{\mu_t}{\sigma_\epsilon} \right) \frac{\partial \epsilon}{\partial z} \right] - C_2 \rho \frac{\epsilon^2}{K} + C_1 \mu_t \frac{\epsilon}{K} \left[2 \left(\frac{\partial U}{\partial x} \right)^2 + 2 \left(\frac{\partial V}{\partial y} \right)^2 + 2 \left(\frac{\partial W}{\partial z} \right)^2 + \left(\frac{\partial U}{\partial y} + \frac{\partial V}{\partial x} \right)^2 + \left(\frac{\partial U}{\partial z} + \frac{\partial W}{\partial x} \right)^2 + \left(\frac{\partial V}{\partial z} + \frac{\partial W}{\partial y} \right)^2 \right] \quad (7)$$

where K is the turbulent kinetic energy term, ϵ is the turbulent energy dissipation term. C_1 and C_2 are constants, whose values are 1.44 and 1.92 for the k- ϵ turbulence model, respectively. Also σ_K (= 1.0 for k- ϵ) and σ_ϵ (= 1.3 for k- ϵ) are turbulent Schmidt numbers. Also the eddy viscosity (μ_t), and eddy conductivity (k_t) can be defined as;

$$\mu_t = C_\mu \rho \frac{K^2}{\epsilon} \quad (8)$$

$$k_t = \frac{\mu_t C_p}{\sigma_t} \quad (9)$$

where σ_t is the turbulent Prandtl number (= 1.0) and C_μ is a constant (= 0.09).

RNG turbulence model is a modified version of the standard model. This model also uses the same equations that standard method uses, except the constant values. In this model, C_1 is a constant, and it is defined as;

$$C_1 = C_0 - \frac{\eta(1-\frac{\eta}{\eta_0})}{1+\beta\eta^3} \quad (10)$$

where η is;

$$\eta = \frac{\sqrt{G}K}{\varepsilon} \quad (11)$$

The G value defined in Equation 11 can be written as;

$$G = 2 \left[\left(\frac{\partial U}{\partial x} \right)^2 + \left(\frac{\partial V}{\partial y} \right)^2 + \left(\frac{\partial W}{\partial z} \right)^2 \right] + \left(\frac{\partial U}{\partial y} + \frac{\partial V}{\partial x} \right)^2 + \left(\frac{\partial U}{\partial z} + \frac{\partial W}{\partial x} \right)^2 + \left(\frac{\partial V}{\partial z} + \frac{\partial W}{\partial y} \right)^2 \quad (12)$$

Other terms that are used for RNG turbulence model are; $C_\mu = 0.085$, $C_0 = 1.42$, $C_2 = 1.68$, $\beta = 0.015$, $\eta_0 = 4.38$, $\sigma_K = 0.7179$ and $\sigma_\varepsilon = 0.7179$.

For the LowRe turbulence model TKE and TED equations are modified by adding a viscosity term (μ) which take the form;

$$\rho \frac{\partial K}{\partial t} + \rho U \frac{\partial K}{\partial x} + \rho V \frac{\partial K}{\partial y} + \rho W \frac{\partial K}{\partial z} = \frac{\partial}{\partial x} \left[\left(\frac{\mu_t}{\sigma_K} + \mu \right) \frac{\partial K}{\partial x} \right] + \frac{\partial}{\partial y} \left[\left(\frac{\mu_t}{\sigma_K} + \mu \right) \frac{\partial K}{\partial y} \right] + \frac{\partial}{\partial z} \left[\left(\frac{\mu_t}{\sigma_K} + \mu \right) \frac{\partial K}{\partial z} \right] - \rho \varepsilon + \mu_t \left[2 \left(\frac{\partial U}{\partial x} \right)^2 + 2 \left(\frac{\partial V}{\partial y} \right)^2 + 2 \left(\frac{\partial W}{\partial z} \right)^2 + \left(\frac{\partial U}{\partial y} + \frac{\partial V}{\partial x} \right)^2 + \left(\frac{\partial U}{\partial z} + \frac{\partial W}{\partial x} \right)^2 + \left(\frac{\partial V}{\partial z} + \frac{\partial W}{\partial y} \right)^2 \right] \quad (13)$$

$$\rho \frac{\partial \varepsilon}{\partial t} + \rho U \frac{\partial \varepsilon}{\partial x} + \rho V \frac{\partial \varepsilon}{\partial y} + \rho W \frac{\partial \varepsilon}{\partial z} = \frac{\partial}{\partial x} \left[\left(\frac{\mu_t}{\sigma_\varepsilon} + \mu \right) \frac{\partial \varepsilon}{\partial x} \right] + \frac{\partial}{\partial y} \left[\left(\frac{\mu_t}{\sigma_\varepsilon} + \mu \right) \frac{\partial \varepsilon}{\partial y} \right] + \frac{\partial}{\partial z} \left[\left(\frac{\mu_t}{\sigma_\varepsilon} + \mu \right) \frac{\partial \varepsilon}{\partial z} \right] - C_2 \rho \frac{\varepsilon^2}{K} + C_1 \mu_t \frac{\varepsilon}{K} \left[2 \left(\frac{\partial U}{\partial x} \right)^2 + 2 \left(\frac{\partial V}{\partial y} \right)^2 + 2 \left(\frac{\partial W}{\partial z} \right)^2 + \left(\frac{\partial U}{\partial y} + \frac{\partial V}{\partial x} \right)^2 + \left(\frac{\partial U}{\partial z} + \frac{\partial W}{\partial x} \right)^2 + \left(\frac{\partial V}{\partial z} + \frac{\partial W}{\partial y} \right)^2 \right] \quad (14)$$

some constants and terms that are used in these equations are the same as the k- ε model. The terms which are different than the k- ε model in this method are;

$$C_\mu = C_{\mu\infty} e^{\frac{-0.25}{(1+R_t/50)}} \quad (15)$$

$$C_2 = C_{2\infty} \left[1 - 0.3e^{-R_t^2} \right] \quad (16)$$

where $C_{\mu\infty}$ and $C_{2\infty}$ are C_μ and C_2 values for the high Reynolds number turbulence model, respectively. Also the turbulence Reynolds number (R_t) value is defined as;

$$R_t = \frac{\rho K^2}{\mu \varepsilon} \quad (17)$$

LowRe turbulence model in Autodesk CFD does not use the wall functions, therefore it is recommended to use more than five levels of wall layer [32]. In order to check this for this turbulence model, three levels of wall layer cell simulation is also investigated in the further sections.

In the comparison of the turbulence models eight different hours were simulated and their outlet temperature values are investigated as the comparison parameter. In order to add all these points into the comparison the average of the deviations of the results from the experimental values given in the literature [28]. This is defined as;

$$D_{avg} = \frac{\sum |T_i - T_{exp_i}|}{n} \quad (18)$$

where T_i is the simulated outlet temperature, T_{exp_i} experimentally measured outlet temperature for that hour in the literature and n is the number of hours that are simulated. It is accepted that, the lower the deviation average, the better the model is.

3. Problem Definition

The numerical setup is defined according to the experimental setup used in the study of Kalaiarasi et al. [28]. This setup is composed of a simple flat plate SAH whose dimensions are given in Figure 1. Since the experiment is made in Madurai/India ($9^{\circ} 56' N$; $78^{\circ} 7' E$; GMT 5.5) on 2nd of June, all the test cases were made with respect to this location and day of the year.

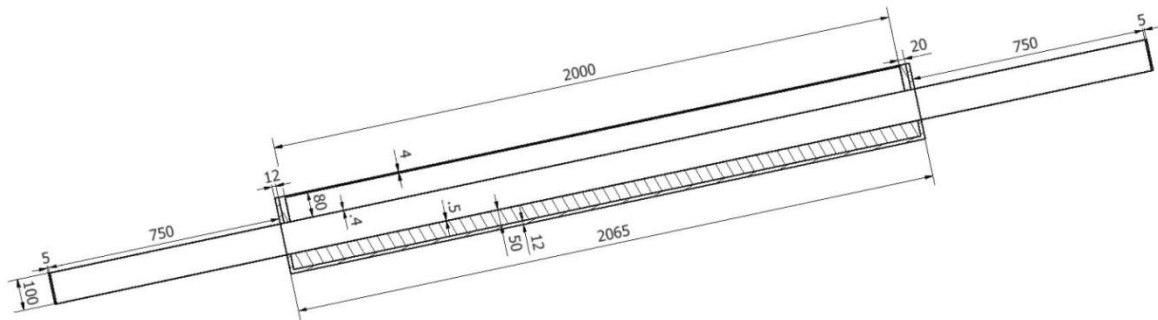


Figure 1. Full section of the numerical model

Three-dimensional model of the SAH used in the simulations is located to the south making an angle of 12° with respect to the ground surface as it is given in Figure 2. Boundary conditions, materials that are used in the SAH were also given in the same figure. The film coefficients were calculated by Designbuilder software and are given in the studies made by Erol [33, 34]. In the design of the SAH, extra inlet and outlet volumes having entrance lengths of 5 mm were added to the model in order to get stable results.

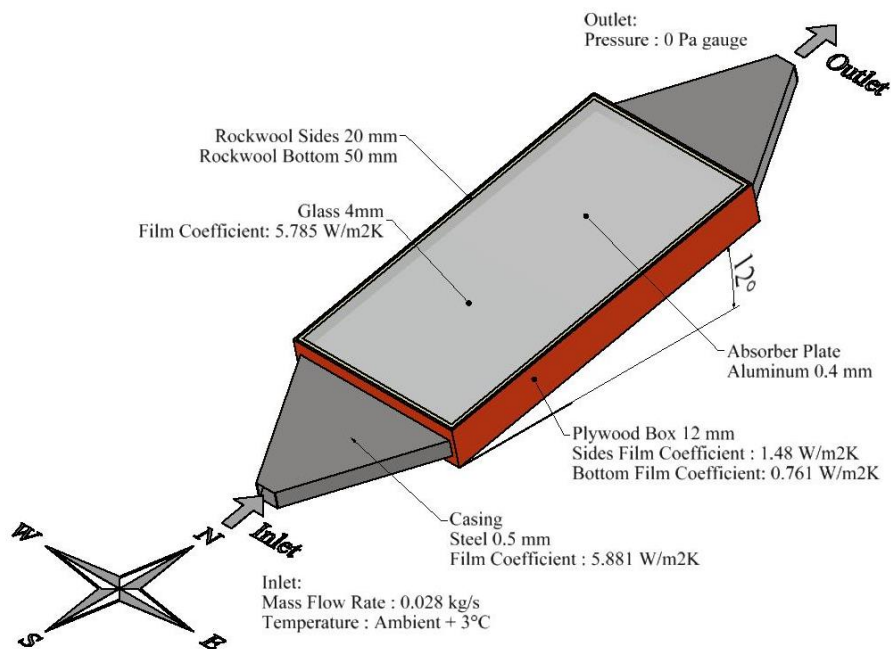


Figure 2. Numerical setup, materials and boundary conditions

In the inlet part of the SAH, inlet boundary condition is defined as mass flow rate of 0.028 kg/s, whose temperature is always 3°C higher than the ambient temperature for each test case. In the simulation of the results steady state calculations were made for every hour between 10:00 and 16:00. For each of the tests, 3, 6 and 9 layers of wall layers were used for each turbulence model as it is given in Figure 3.

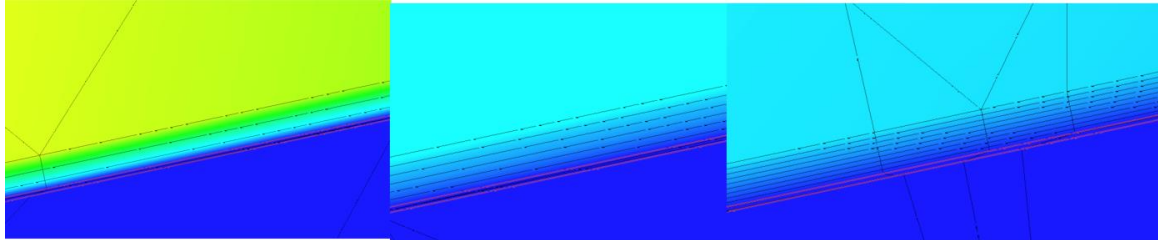


Figure 3. 3, 6 and 9 levels of wall layer

4. Results

In this section, the results that were acquired from the CFD simulations for each turbulence models were presented and the comparisons were made between the experimental results and the simulated values. In the first three subsections, mesh dependence tests and the outlet temperature results for different wall layer thickness of the same models were presented.

In the next section, best results that were selected from these methods were compared separately and the other parameters like the streamlines and the temperature distributions in the flow were investigated.

4.1. k-ε Method

In the mesh dependence tests of this study, the solution is considered to be accepted as mesh independent if the control parameter changes about 1% for a node number increase of over 50% [33]. In this study, outlet temperature of the SAH is accepted as the control parameter. After a series of simulations, outlet temperatures for different node numbers of each wall layer cell number were acquired. The change in outlet temperature with respect to the node number is given in Figure 4. The results that were acquired from the simulations showed that for 3, 6 and 9 levels of wall layer thicknesses of the k-ε turbulence model, 30487, 44635 and 58796 nodes were selected for the rest of the simulations, respectively.

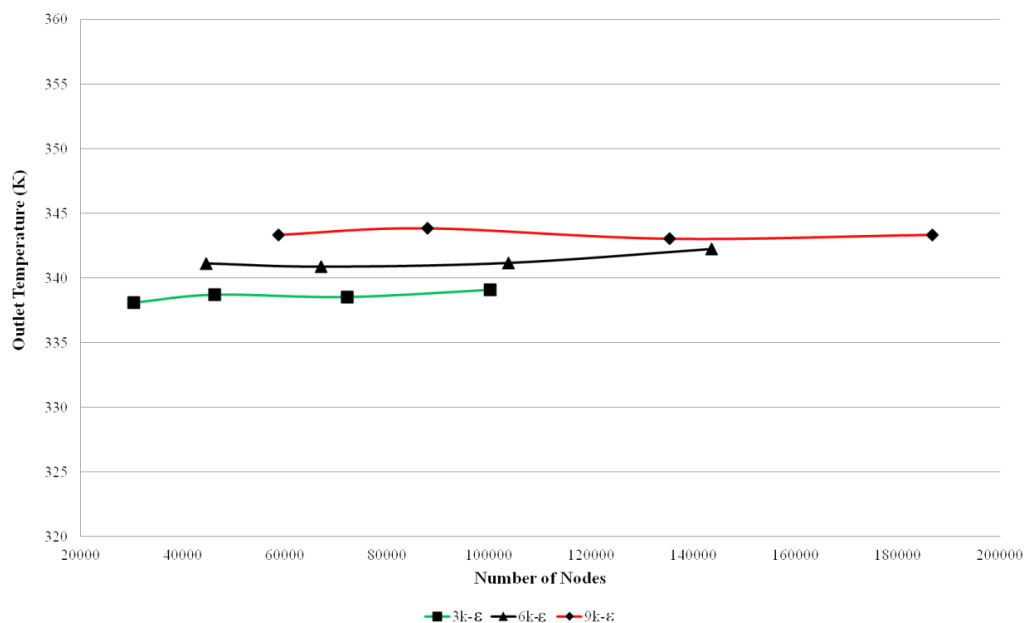


Figure 4. Outlet Temperature vs. Node Number for k-ε

Figure 5 and Table 1 shows the outlet temperature of the reference experimental study [28] and the simulation results of $k-\epsilon$ turbulence model for three different wall layers. The average deviation from the experimental results for 3, 6 and 9 layers of wall layer thickness were found as 3.77, 4.22 and 4.42 K. According to the results, 3 $k-\epsilon$ simulation has the lowest deviation average compared to the experimental results. Therefore, it can be said that three layers can be accepted as the best wall layer value for the $k-\epsilon$ turbulence model for this problem.

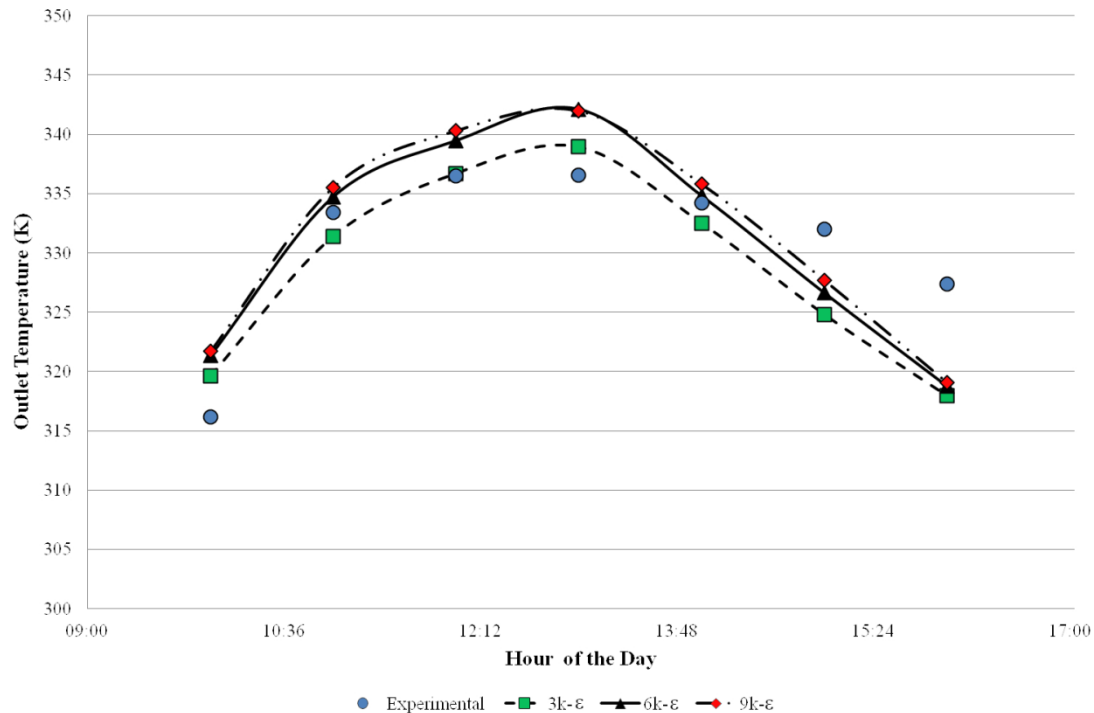


Figure 5. Comparison of outlet temperatures of $k-\epsilon$ model of three different levels of wall layers with experimental [28] results

Table 1. Comparison of outlet temperatures of $k-\epsilon$ model of three different levels of wall layers with experimental [28] results and ambient conditions

Hour	Irradiation (W/m ²)	Inlet Temp (K)	Ambient	Experimental (K)[20]	3k-ε (K)	6k-ε (K)	9k-ε (K)
10:00	518.39	308.77	305.769	316.18	319.65	321.34	321.71
11:00	788.13	311.05	308.049	333.44	331.41	334.74	335.53
12:00	853.85	312.67	309.665	336.53	336.71	339.47	340.3
13:00	818.75	316.35	313.348	336.58	338.93	342.12	341.97
14:00	695.91	316.1	313.102	334.25	332.51	334.82	335.81
15:00	573.57	313.6	310.587	331.99	324.82	326.63	327.7
16:00	476.01	311.7	308.714	327.4	317.97	318.75	319.08

4.2. Low Reynolds $k-\epsilon$ Method

For the Low Reynolds $k-\epsilon$ turbulence model, Figure 6 shows the mesh dependence test. According to the results that were acquired, for 3, 6 and 9 levels of wall layers, 30487, 44635 and 87867 nodes are accepted as mesh independent test cases, respectively. Since this turbulence model do not use wall functions, wall layer numbers lower than five layers is not recommended [32], but in order to see the effect, a three layer solution was also added to the investigation.

For these node numbers, using LowRe turbulence model for three different levels of wall layers, results that were given in Figure 7 and Table 2 was acquired. Average deviations for this turbulence model for 3, 6 and 9 levels of wall layers were calculated as 7.94, 4.01 and 4.56 K, respectively. These results make the 6LowRe as the best solution for the LowRe turbulence model.

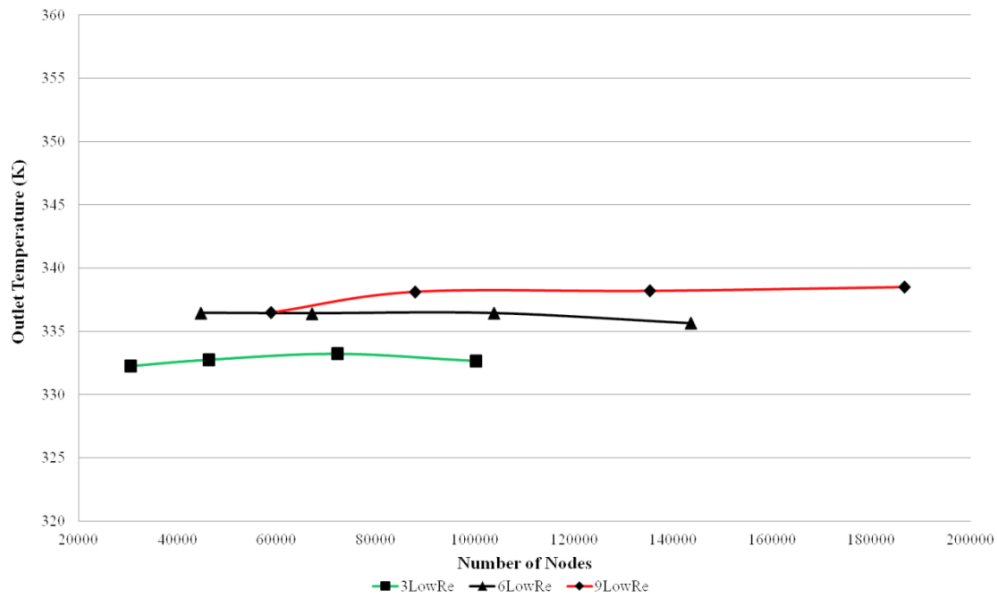


Figure 6. Outlet Temperature vs. Node Number for LowRe

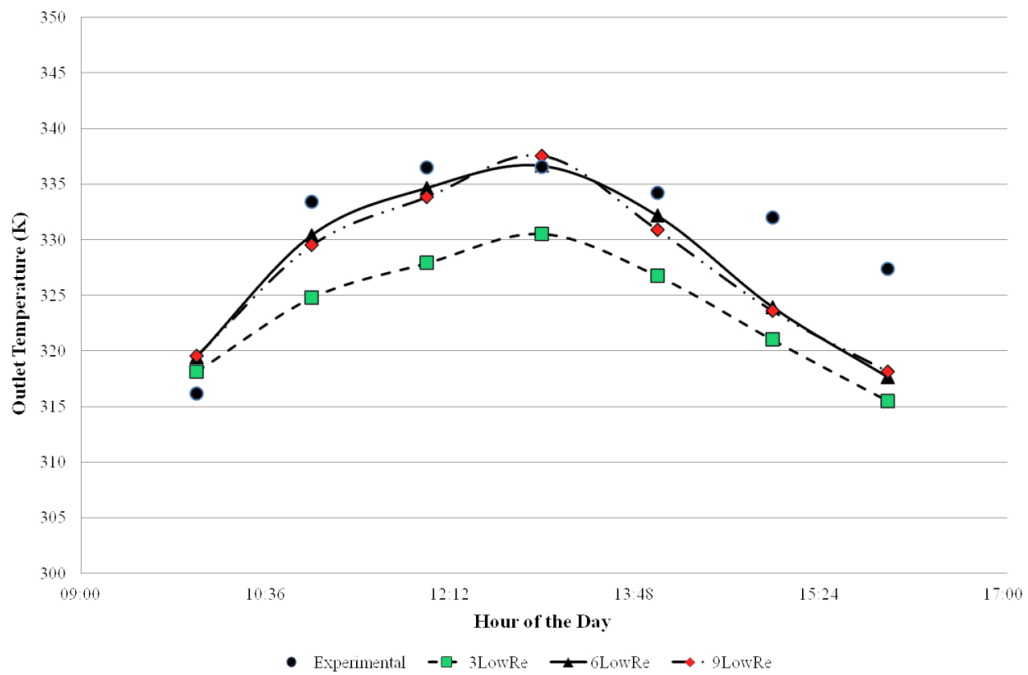


Figure 7. Comparison of outlet temperatures of LowRe for three different levels of wall layers with experimental [28] results

Table 1. Comparison of outlet temperatures of LowRe model of three different levels of wall layers with experimental [28] results and ambient conditions

Hour	Irradiation (W/m ²)	Inlet Temp (K)	Ambient	Experimental (K)[20]	3LowRe (K)	6LowRe (K)	9LowRe (K)
10:00	518.39	308.77	305.77	316.18	318.14	319.45	319.57
11:00	788.13	311.05	308.05	333.44	324.79	330.43	329.51
12:00	853.85	312.67	309.67	336.53	327.91	334.68	333.85
13:00	818.75	316.35	313.35	336.58	330.54	336.66	337.56
14:00	695.91	316.1	313.1	334.25	326.76	332.18	330.91
15:00	573.57	313.6	310.6	331.99	321.01	323.95	323.62
16:00	476.01	311.71	308.71	327.4	315.52	317.65	318.18

4.3. RNG k- ϵ Method

For the RNG turbulence model, mesh dependence tests are given in Figure 8. According to the simulations, for 3, 6 and 9 levels of wall layers, 46260, 67071 and 87867 nodes are accepted as mesh independent for the test cases, respectively.

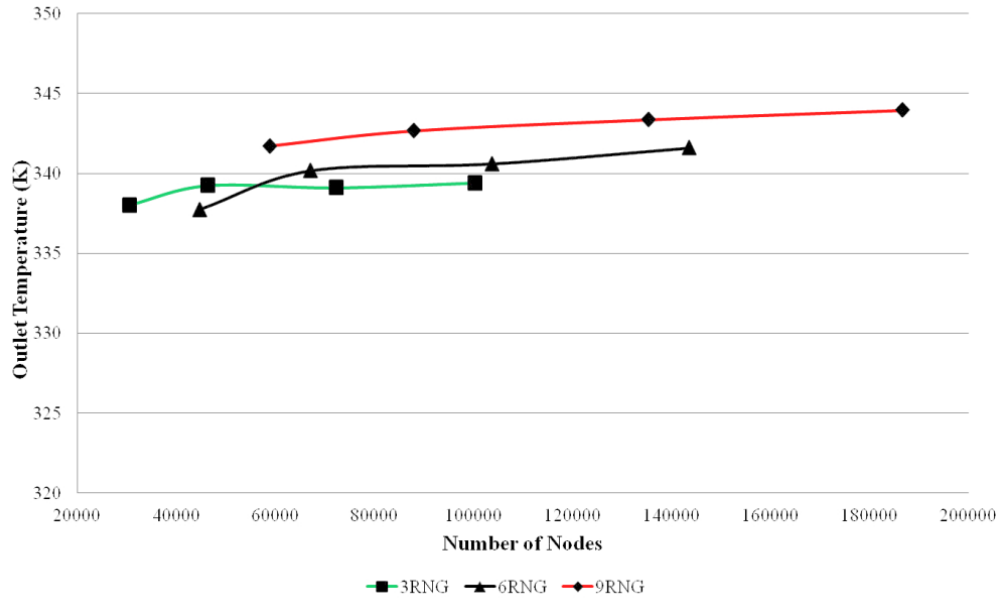


Figure 8. Outlet Temperature vs. Node Number for RNG

By using these node numbers for each wall layer thickness, solar calculations were made between hours 10:00 and 16:00. According to the simulations that were made, results were given in Figure 9 and Table 3. The average deviations of 3, 6 and 9 levels of wall layer for the RNG model were calculated as 4.07, 3.41 and 4.73K, respectively. The lowest average deviation value for RNG was found to be the six layers of wall layer thickness.

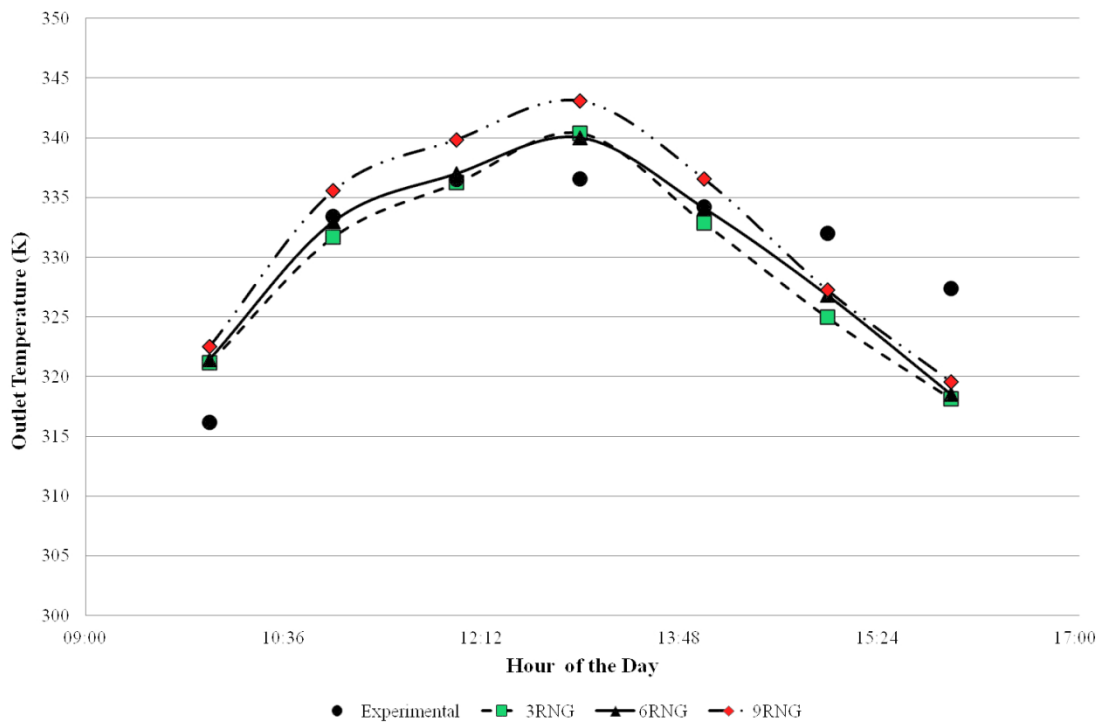


Figure 9. Comparison of outlet temperatures of RNG for three different levels of wall layers -with experimental [28] results

Table 3. Comparison of outlet temperatures of LowRe model of three different levels of wall layers with experimental [28] results and ambient conditions

Hour	Irradiation (W/m ²)	Inlet Temp (K)	Ambient	Experimental (K)[20]	3RNG (K)	6RNG (K)	9RNG (K)
10:00	518.39	308.77	305.77	316.18	321.16	321.44	322.53
11:00	788.13	311.05	308.05	333.44	331.67	332.98	335.55
12:00	853.85	312.67	309.67	336.53	336.24	337.02	339.85
13:00	818.75	316.35	313.35	336.58	340.39	340.04	343.08
14:00	695.91	316.10	313.10	334.25	332.89	334.13	336.56
15:00	573.57	313.59	310.59	331.99	324.96	326.81	327.26
16:00	476.01	311.71	308.71	327.4	318.17	318.49	319.59

4.4. Computation Cost of the Turbulence Models

For every analysis, different turbulence models with different wall layer levels results in different number of iterations to convergence. Also this change the analysis time required to get a converged solution. Method and the node numbers used in the solution are the two main factors that are affecting the computation costs. Table 4 shows the node numbers that are used in the comparison process. The higher the node number the longer the iteration time is.

Table 4. Node numbers used in the comparison process calculations

	3k- ϵ	6k- ϵ	9k- ϵ	3LowRe	6LowRe	9LowRe	3RNG	6RNG	9RNG
Node Number	30487	44635	58796	30487	44635	87867	46260	67071	87867
% difference wrt. 3k-ϵ node number	-	46,41	92,86	0,00	46,41	188,21	51,74	120,00	188,21

But the node number is not the only parameter. The calculation method and the formulations that are used is also an important parameter in the computational cost. Figure 10 shows the iteration number and analysis time required for convergence of the solution at 13:00. When these results were studied it can be said that LowRe turbulence model has the biggest iteration numbers and the analysis time. Although RNG method has a computation cost similar to the LowRe turbulence model, because of the shorter convergence iterations its cost seems lower than the LowRe turbulence model.

k- ϵ turbulence model has the lowest computation cost among the turbulence models that were compared. Not only the mesh independent node number is the lowest, but also the analysis time is lower than the other two turbulence models, even if the convergence iteration number is higher than the RNG turbulence method.

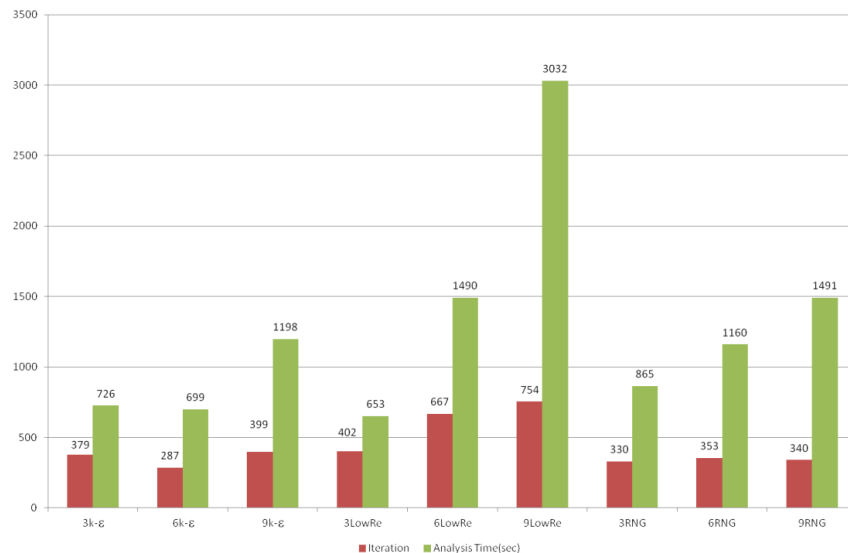


Figure 10. Iteration and analysis time to convergence of turbulence models for 3, 6 and 9 levels of wall layer at 13:00.

4.5. Comparison of Turbulence Models

In this section, since the best results were acquired from these wall layer levels, comparison of 3k- ϵ , 6LowRe and 6RNG cases were made. Figure 11 shows the results that were acquired by the simulations and the experimental results that are in the literature for eight hours of the day beginning from 10:00 until 16:00. According to the deviation average values for each of these turbulence model it is found that 6RNG turbulence model is the best choice among these three turbulence layers.

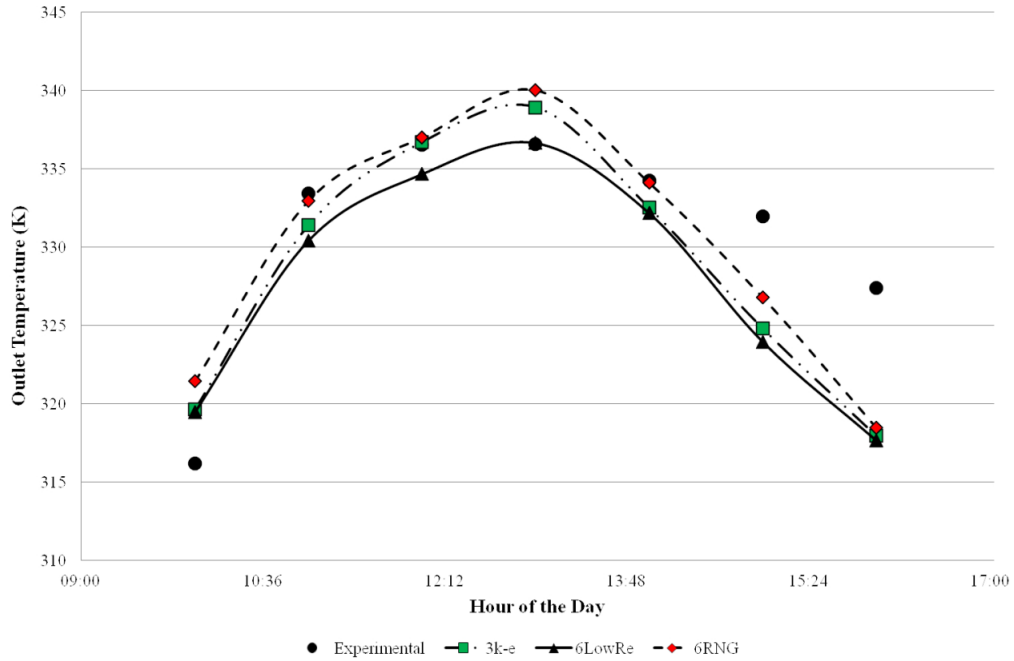


Figure 11. Comparison of outlet temperatures of three turbulence model with experimental [28] results

Figures 12, 13 and 14 show the streamlines and the temperature contours of the flow in the SAH for 10:00, 13:00 and 16:00 hours. These three hours were selected in order to see the effect of the sun in the east, azimuth and west. When the streamlines were investigated it can be seen that for every model the flow begins as a jet and the flow then distributes in the channel. This distribution is more visible for the 6RNG model. When it is compared with the RNG model, distribution of the streamlines for the k- ϵ and LowRe models are very small and concentrated on the outlet side.

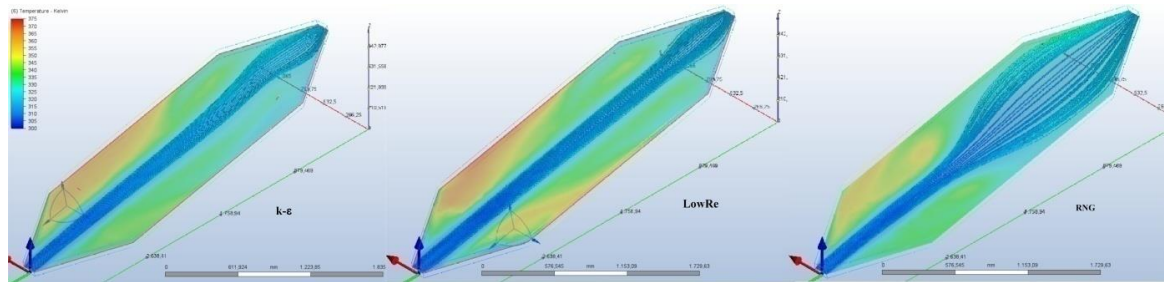


Figure 12. Temperature contours and streamlines for different turbulence models on 10:00

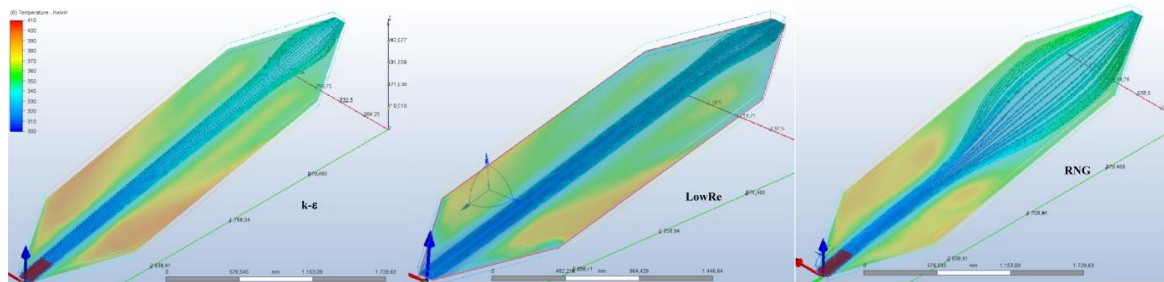


Figure 13. Temperature contours and streamlines for different turbulence models on 13:00

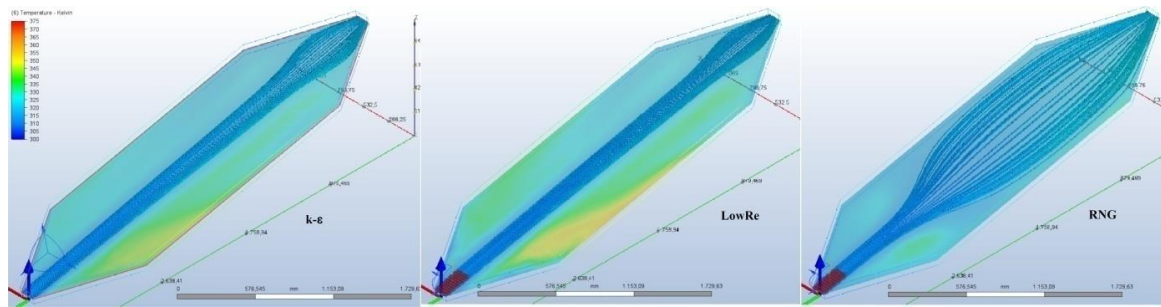


Figure 14. Temperature contours and streamlines for different turbulence models on 16:00

Because of this distribution, 6RNG model found higher outlet temperature values compared to the other turbulence models. Especially for 11:00, 12:00 and 14:00, this method is in a good agreement with the experimental values given in the literature, compared with the other turbulence models.

5. Discussion and Conclusion

With this study, the effect of three turbulence models and three wall layer thicknesses on each of these models were investigated on a flat plate SAH. Calculations were made by using Autodesk CFD software and radiation calculations were added to the simulations. After investigating the results that were acquired from the simulations, following conclusions can be reached;

- Using more wall layer does not guarantee the successful simulation results.
- k- ϵ method has the lowest computation cost among all other turbulence models.
- Worst results were acquired by using LowRe turbulence model with 3 layers of wall layer mesh structure as it is expected.
- Although 3k- ϵ and 6RNG have nearly the same daily average deviation, on hourly basis RNG model calculates the outlet temperature much closer than the k- ϵ method.

When one focuses on the hourly simulations, 6RNG method is found to be the best method in this study. But when the computation cost is added to the comparison parameters it can be said that k- ϵ turbulence model with three levels of wall layer can be chosen as a better alternative than RNG turbulence model with six levels of wall layer.

Conflict of Interest Statement

The author declare that there is no conflict of interest

References

- [1] P. Mishra and K. Aharwal, "A review on selection of turbulence model for CFD analysis of air flow within a cold storage," *IOP Conf. Ser.: Mater. Sci. Eng.*, vol. 402, pp. 012145, September 2018. doi:10.1088/1757-899X/402/1/012145
- [2] Y. Bartosiewicz, Z. Aidoun, P. Desevaux and Y. Mercadier, "CFD-Experiments Integration in the Evaluation of Six Turbulence Models for Supersonic Ejectors Modeling," 2004. [Online]. Available: http://cfd4aircraft.com/int_conf/IC1/papers/Bartosiewicz.pdf. [Accessed: February,03,2022].
- [3] J. Gagan, K. Smierciew, D. Butrymowicz and J. Karwacki, "Comparative study of turbulence models in application to gas ejectors," *International Journal of Thermal Sciences*, vol 78, pp. 9-15, 2014. doi:10.1016/j.ijthermalsci.2013.11.009
- [4] S. Varga, J. Soares, R. Lima and A. Oliveira, "On the Selection of a Turbulence Model for the Simulation of Steam Ejectors Using CFD," *International Journal of Low-Carbon Technologies*, vol. 12, no. 3, pp. 233-243, June 2017. doi:10.1093/ijlct/ctx007
- [5] M. Bulat and P. Bulat, "Comparison of Turbulence Models in the Calculation of Supersonic Separated Flows," *World Applied Sciences Journal*, vol. 27, no. 10, pp. 1263-1266, January 2013. doi:10.5829/idosi.wasj.2013.27.10.13715
- [6] D. Monk and E. Chadwick, "Comparison of Turbulence Models Effectiveness for a Delta Wing at Low Reynolds Numbers," in *7th european conference for aeronautics and space sciences, Eucass*, July, 03-07, 2017, Milan, Italy [Online]. Available: <https://www.eucass.eu/doi/EUCASS2017-653.pdf> [Accessed: February, 22, 2022]. doi:10.13009/EUCASS2017-653
- [7] S. Aftab, A. Rafie, N. Razak and K. Ahmad, "Turbulence Model Selection for Low Reynolds Number Flows," *PLoS ONE*, vol 11,

no. 4, pp. e0153755, 2016. doi:10.1371/journal.pone.0153755

[8] K. Bharanitharan, S. Senthilkumar and B. Dadhich, "Numerical Investigation on Effect of Turbulence Model Selection for Aerodynamic Prediction of Axial Flow Fan," *IOP Conf. Ser.: Mater. Sci. Eng.*, vol. 1130, no. 1, p. 012055, 2021. doi:10.1088/1757-899X/1130/1/012055

[9] R. Tog, A. Tousi and A. Tourani, "Comparison of Turbulence Methods in CFD Analysis of Compressible Flows in Radial Turbomachines," *Aircraft Engineering and Aerospace Technology: An International Journal*, vol. 80, no. 6, pp. 657-665, 2008. doi:10.1108/00022660810911608

[10] L. Gibson, L. Galloway, S. i. Kim and S. Spence, "Assessment of Turbulence Model Predictions for a Centrifugal Compressor Simulation," *Journal of the Global Power and Propulsion Society*, vol. 1, pp. 142-156, 2017. doi:10.22261/JGPPS.2II890

[11] L. Han and P. Huachen, "The Influence of Turbulence Model Selection and Leakage Considerations on CFD Simulation Results for a Centrifugal Pump," *Advanced Materials Research*, vols. 594-597, pp. 1940-1944, November, 2012. doi:10.4028/www.scientific.net/AMR.594-597.1940

[12] A. Rezaeiha, H. Montazeri and B. Blocken, "On the Accuracy of Turbulence Models for CFD Simulations of Vertical Axis Wind Turbines," *Energy*, vol. 180, pp. 838-857, May 2019. doi:10.1016/j.energy.2019.05.053

[13] A. Meana-Fernandez, J. Oro, K. Diaz and S. Velarde-Suarez, "Turbulence-Model Comparison for Aerodynamic-Performance Prediction of a Typical Vertical-Axis Wind-Turbine Airfoil," *Energies*, vol. 12, no. 3, pp. 488, February, 2019. doi:10.3390/en12030488

[14] P. Marsh, D. Ranmuthugala, I. Penesis and G. Thomas, "The Influence of Turbulence Model and Two and Three-Dimensional Domain Selection on the Simulated Performance Characteristics of Vertical Axis Tidal Turbines," *Renewable Energy*, vol. 105, pp. 106-116, December, 2017. doi:10.1016/j.renene.2016.11.063

[15] M.-H. Kim, N.-i. Tak and J.-M. Noh, "Study on Influence of Turbulence Model Selection on Prediction of Flow Distribution and Hot Spot Fuel Temperature in Prismatic HTGR Cores," *Engineering Applications of Computational Fluid Mechanics*, vol. 8, no. 2, pp. 263-273, November, 2014. doi:10.1080/19942060.2014.11015512

[16] A. Guardo, M. Coussirat, M. Larrayoz, F. Recasens and E. Egusquiza, "Influence of the Turbulence Model in CFD Modeling of Wall-to-Fluid Heat Transfer in Packed Beds," *Chemical Engineering Science*, vol. 60, no. 6, pp. 1733-1742, January, 2005. doi:10.1016/j.ces.2004.10.034

[17] G. Brown, D. Fletcher, J. Leggoe and D. Whyte, "Investigation of the Turbulence Model Selection on the Predicted Flow Behaviour in and Industrial Crystallizer - RANS and URANS Approaches," *Chemical Engineering Research and Design*, vol. 140, pp. 205-220, October, 2018. doi:10.1016/j.cherd.2018.10.007

[18] F. Mirzaei, F. Mirzaei and E. Kashi, "Turbulence Model Selection for Heavy Gases Dispersion Modeling in Topographically Complex Area," *Journal of Applied Fluid Mechanics*, vol. 12, no. 6, pp. 1745-1755, November, 2019. doi:10.29252/jafm.12.06.29685

[19] Autodesk, "Wall Layers", May 27, 2021. [Online]. Available: <https://knowledge.autodesk.com/support/cfd/learn-explore/caas/CloudHelp/cloudhelp/2021/ENU/SimCFD-UsersGuide/files/The-CFD-Process/Setup-Tasks/Meshing/GUID-F9C4DDB4-8111-4F25-8EDE-D7C38B3BAD99-html.html>. [Accessed: May, 04, 2022].

[20] M. Vivekanandan, D. Jagadeesh, A. Natarajan, N. Mohan and M. Dineshkumar, "Experimental and CFD Investigation of Fully Developed Flow Solar Air Heater," *Materials Today: Proceedings*, vol. 37, part 2, pp. 2158-2163, 2021. doi:10.1016/j.matpr.2020.07.638

[21] A. P. Singh, A. Kumar, Akshayveer and O. P. Singh, "Natural Convection Solar Air Heater: Bell-Mouth Integrated Converging Channel for High Flow Applications," *Building and Environment*, vol. 187, pp. 107367, January 2021. doi:10.1016/j.buildenv.2020.107367

[22] A. P. Singh, A. Kumar, Akshayveer and O. P. Singh, "Effect of Integrating High Flow Naturally Driven Dual Solar Air Heaters with Trombe Wall," *Energy Conversion and Management*, vol. 249, pp. 114861, December 2021. doi:10.1016/j.enconman.2021.114861

[23] A. Kumar, A. P. Singh, Akshayveer and O. P. Singh, "Performance Characteristics of a New Curved Double-Pass Counter Flow Solar Air Heater", *Energy*, vol. 239, part A, pp. 121886, January 2022. doi:10.1016/j.energy.2021.121886

[24] K. D. Yadav and R. K. Prasad, "Performance Analysis of Parallel Flow Flat Plate Solar Air Heater Having Arc Shaped Wire Roughened Absorber Plate," *Renewable Energy Focus*, vol. 32, pp. 23-44, March 2020. doi:10.1016/j.ref.2019.10.002

[25] R. Kumar and V. Goel, "Unconventional Solar Air Heater with Triangular Flow-Passage: A CFD Based Comparative Performance Assessment of Different Cross-Sectional Rib-Roughnesses," *Renewable Energy*, vol. 172, pp. 1267-1278, July 2021. doi:10.1016/j.renene.2021.03.068

[26] Z. Zhao, L. Luo, D. Qui, Z. Wang and B. Sundén, "On the Solar Air Heater Thermal Enhancement and Flow Topology Using Differently Shaped Ribs Combined with Delta-Winglet Vortex Generators," *Energy*, vol. 224, pp. 119944, June 2021. doi:10.1016/j.energy.2021.119944

- [27] K. Saurabh and H. Thakur, "Heat Transfer and Fluid Flow Analysis of Artificially Roughened Solar Air Heater," *Materials Today: Proceedings*, vol. 56, part 2, pp. 910-920, 2022. doi:10.1016/j.matpr.2022.02.540
- [28] G. Kalaiarasi, R. Verlaj, M. Vanjeswaran and N. Pandian, "Experimental Analysis ana Comparison of Flat Plate Solar Air Heater with and without Integrated Sensible Heat Storage," *Renewable Energy*, vol. 150, no. 6, pp. 255-265, May 2020. doi:10.1016/j.renene.2019.12.116
- [29] Autodesk, "General Fluid Flow and Heat Transfer Equations," December, 09, 2019. [Online]. Available: <https://knowledge.autodesk.com/support/cfd/learn-explore/caas/CloudHelp/cloudhelp/2014/ENU/SimCFD/files/GUID-83A92AE5-0E9E-4E2D-B61F-64B3696E5F66-htm.html>. [Accessed: February, 15, 2022].
- [30] Autodesk, "Turbulent Flow," Autodesk, December, 09, 2019. [Online]. Available: <https://knowledge.autodesk.com/support/cfd/learn-explore/caas/CloudHelp/cloudhelp/2014/ENU/SimCFD/files/GUID-BBA4E008-8346-465B-9FD3-D193CF108AF0-htm.html>. [Accessed: February, 21, 2022].
- [31] Autodesk, "Two Equation Turbulence Models (TKE & TED)," Autodesk, May 27, 2021. [Online]. Available: <https://knowledge.autodesk.com/support/cfd/learn-explore/caas/CloudHelp/cloudhelp/2021/ENU/SimCFD-Learning/files/Reference-Material/Theoretical-Background/Governing-Equations/Turbulent-Flow/GUID-61C4EB55-362C-48A0-8B22-20F9148D190D-html.html>. [Accessed: February, 20, 2022].
- [32] Autodesk, "Turbulence, CFD 2021," May 27, 2021. [Online]. Available: <https://knowledge.autodesk.com/support/cfd/learn-explore/caas/CloudHelp/cloudhelp/2021/ENU/SimCFD-UsersGuide/files/The-CFD-Process/Solving-the-Simulation/Solve-Quick-Edit-dialog-Physics/GUID-E9E8ACA1-8D49-4A49-8A35-52DB1A2C3E5F-html.html>. [Accessed: February, 14, 2022].
- [33] Ö. Erol, "Numerical Investigation of the Fins and Turbulators on the Performance of a Solar Air Heater", in *23rd Congress on Thermal Science and Technology with International Participation, ULIBTK 2021*, September, 08-10, 2021, Gaziantep, Turkey, N. Yücel, R. Yumrutaş, M.S. Söylemez, M. Kanoğlu, A. Atmaca, H. Yağlı, Eds., pp. 502-509.
- [34] Ö. Erol, "Analysis of the Performance of a Solar Air Heater with Different Configurations: Effect of Fins and Turbulators," *Heat Transfer Research*, vol. 53, no. 6, pp. 45-39, March 2022. doi:10.1615/HeatTransRes.2022041666

This is an open access article under the CC-BY license

